JNAOE
©SNAK, 2009

Inter J Nav Archit Oc Engng (2009) 1:1~12
http://dx.doi.org/10.2478/IJNAOE-2013-0001

Aerodynamic characteristics of NACA 4412 airfoil section with flap in extreme ground effect

Alex E. Ockfen and Konstantin I. Matveev

School of Mechanical and Materials Engineering, Washington State University, Pullman, WA, 99164-2920,

ABSTRACT: *Wing-in-Ground vehicles and aerodynamically assisted boats take advantage of increased lift and reduced drag of wing sections in the ground proximity. At relatively low speeds or heavy payloads of these craft, a flap at the wing trailing-edge can be applied to boost the aerodynamic lift. The influence of a flap on the two-dimensional NACA 4412 airfoil in viscous ground-effect flow is numerically investigated in this study. The computational method consists of a steady-state, incompressible, finite volume method utilizing the Spalart-Allmaras turbulence model. Grid generation and solution of the Navier-Stokes equations are completed using computer program Fluent. The code is validated against published experimental and numerical results of unbounded flow with a flap, as well as ground-effect motion without a flap. Aerodynamic forces are calculated, and the effects of angle of attack, Reynolds number, ground height, and flap deflection are presented for a split and plain flap. Changes in the flow introduced with the flap addition are also discussed. Overall, the use of a flap on wings with small attack angles is found to be beneficial for small flap deflections up to 5% of the chord, where the contribution of lift augmentation exceeds the drag increase, yielding an augmented lift-to-drag ratio.*

***KEY WORDS**:* Ground effect; Flap; Airfoil; NACA 4412; CFD; Fluent.

INTRODUCTION

High-speed, high-payload marine and amphibious transportation means benefit from using aerodynamic lift enhanced in ground vicinity. Various types of Wing-in-Ground (WIG) craft, mainly experimental, were constructed and tested in the last century (Rozhdestvensky, 2006). The most effective lift increase and drag reduction are obtained in the so-called extreme-ground flight regimes, roughly corresponding to the wing height over the ground surface being about or less than 0.1 of the wing chord. A new generation of aerodynamically assisted transport platforms using Power Augmented Ram (PAR) principle has been under development (Gallington, 1987; Kirillovykh and Privalov, 1996; Matveev, 2008). PAR craft operate in the extreme ground effect and rely on both aerodynamic and jet support. The development of complex ground-effect vehicles is hampered by high costs and accuracy issues in conducting experimental studies. Hence, the application of rapidly advancing CFD methods can help the engineering community make a significant progress in the air-assisted fast transportation.

The Wing-in-Ground effect, taking place when an airfoil flies in close proximity to the ground, provides beneficial aerodynamic properties. As the airfoil altitude approaches one wing span, the wingtip vortices become partly blocked by the ground, reducing the lift-induced drag and increasing lift. Further decreasing the ground height to within a small fraction of the wing chord, corresponding to the extreme ground effect, will trap flow underneath the airfoil, providing a high pressure ram effect which significantly increases the aerodynamic lift. It is apparent that the span-based ground effect is a three-dimensional phenomenon. However, the nearly two-dimensional chord-based effect dominates in the extreme ground proximity, when endplates are employed or large-aspect ratio airfoils are utilized.

Many WIG vehicles are designed to skim above water or a relatively flat solid surface. At low speeds or on heavy-loaded craft a flap is employed at the trailing edge of the airfoil to strongly augment the airfoil lift. By adjusting the flap position, flow around the airfoil can be controlled, in turn providing control of the aerodynamic properties of the airfoil. In many cases where ground height and the wing attack angle are relatively fixed, a flap can be used to regulate the aerodynamic lift of the vehicle in ground vicinity.

A variety of inviscid numerical methods have been applied in the past for calculating ground-effect flows and even simulating dynamics of WIG craft (Gallington et al., 1976; Katz and Plotkin, 1991; Kornev and Matveev, 2003; Rozhdestvensky, 2000). In recent years, several studies have been published using viscous numerical methods to solve

Corresponding author: *Konstantin I. Matveev*
e-mail: *matveev@wsu.edu.*

two-dimensional incompressible flows around airfoils in ground effect. A finite volume method employing the k-ε turbulence model was used on an NACA 4412 airfoil by Hsiun and Chen (1996) along with a fixed ground boundary condition. They concluded that a decrease in lift was found in the extreme ground effect due to the boundary layer created between the fixed ground and free stream flow. Different ground boundary conditions on the NACA 4412 airfoil were studied by Barber et al. (1998). They note that the fixed ground condition is unrealistic for WIG craft, and propose the use of a moving ground at the free stream speed. A finite difference scheme and the Baldwin-Lomax turbulence model are used by Chun and Chang (2003) in their investigation of the fixed and moving ground conditions for an NACA 4412 airfoil. Again, they also see a significant difference between a fixed and moving ground. All of the above numerical models, which use the moving ground boundary condition, predict an increase in lift during ground-effect flight, although there is some variation in the magnitude of predicted forces. A few modeling analyses of three-dimensional WIG configurations by viscous solvers were also accomplished (Hirata and Hino, 1997; Wu and Rozhdestvensky, 2001).

Experimental data for wing sections in proximity to fixed ground and moving ground are available in the literature (Hayashi and Endo, 1978). These data correspond to flow of Reynolds number on the order of 10^5. At these Reynolds numbers the flow is known to be generally laminar on a significant portion of the chord, which makes it difficult to extrapolate such data even for small WIG craft. Kikuchi et al. (2002) present results obtained on a NACA 4412 airfoil towed at a Reynolds number of 8×10^5. Although the flow is still below the general WIG operating range, practical aerodynamic trends are obtained. They conclude that the ground effect augments the lift in all cases in which geometry does not create the Venturi effect below the airfoil.

Little published research has been found for the use of a flap in the extreme proximity to the ground. Most studied configurations were complicated PAR systems (Huffman and Jackson, 1974; Krause, 1997). Serebrisky and Biachev (1946) tested Clark-Y sections by the method of images in this region and found that use of flap in ground effect improves the aerodynamic efficiency for small angles of attack. Numerous experimental data collected by Abbott and Doenhoff (1959) show that a flap can significantly augment the lift in the free airflow. The flap application has been numerically and experimentally studied by Steinbach and Jacob (1991) in the distant ground effect, with height-to-chord ratio from around one quarter to above one. Their numerical technique consisted of a panel method, which was iterated with boundary layer and rear displacement models to account for viscosity and separation. It is concluded that wing systems with excessive flap-slat mechanization are often unfavorable in the distant ground effect as the wing effective camber produces a negative ground effect. Their results also show that as a high-lift airfoil with a flap approaches the ground, the flap efficiency decreases, and the separation point moves further upstream.

However, nearly flat lower airfoil surfaces and moderate flap deflections and attack angles are known to be quite beneficial in ground proximity. The goal of this paper is to investigate favorable trailing-edge flap configurations that improve aerodynamic characteristics of the NACA 4412 wing section in the extreme ground effect. The extreme ground effect region has been chosen as it provides the most beneficial aerodynamic properties for ground-effect vehicles and obtained numerical solutions are generally steady. As a wing with flap moves farther from the ground, unsteady effects begin to take place and an unsteady solution is required. In this work, a numerical study of viscous ground-effect flow is completed using the commercial code Fluent 6.3. The performance of various flap configurations are compared for different ground height, flap deflection, Reynolds number, and angle of attack, providing a beneficial region of flap use in extreme ground effect.

NUMERICAL METHOD

Airfoil geometry

The NACA 4412 airfoil has been studied since its nearly flat bottom surface prevents the negative ground effect that occurs with extreme camber or when Venturi flow is created beneath the airfoil. The NACA 4412 geometry and main parameters of the study are shown in Fig. 1.

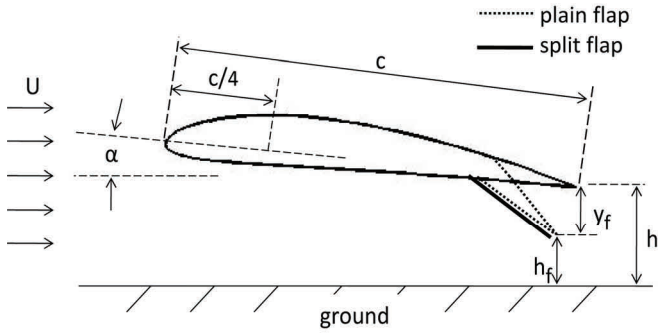

Fig. 1 Schematic for modelling airflow around NACA 4412 wing section with flap in ground effect

The distance from the tip of the flap to the ground is denoted as h_f, while the distance from the trailing edge of the wing section with undeflected flap to the ground is defined as h. The difference between h and h_f represents the total flap deflection, which is denoted as y_f. The angle of attack is defined as the angle between the chord line connecting the leading and trailing edge of the wing without flap and the horizontal plane, while the quarter chord moment coefficient is found with respect to the location on the camber line one quarter of the chord downstream of the leading edge. In the current study, the NACA 4412 airfoil is modified with plain and split flaps which are added at 80% chord. Plain flap configurations deflect the airfoil trailing edge to the specified position while split flap configurations add a thin plate flap beneath the airfoil without deflecting the airfoil trailing edge (Fig. 1).

Numerical model

Turbulent flow is specified over the entire airfoil, similar to other CFD studies of ground-effect wings. The general equations governing the current WIG flow with a flap are the two-dimensional, incompressible, constant viscosity, turbulent Reynolds Averaged Navier Stokes (RANS) equations, consisting of the continuity equation, which represents the conservation of mass, and the momentum equation, representing the conservation of momentum,

$$\frac{\partial}{\partial x_i}\left(u_i\right) = 0 \tag{1}$$

$$\rho\frac{\partial}{\partial t}\left(u_i\right) + \rho\frac{\partial}{\partial x_j}\left(u_i u_j\right) = -\frac{\partial p}{\partial x_i} + \mu\frac{\partial}{\partial x_j}\left(\frac{\partial u_i}{\partial x_j}\right) + \frac{\partial}{\partial x_j}\left(-\rho\left\langle u_i' u_j'\right\rangle\right) \tag{2}$$

where u_i is the ensemble averaged velocity in the *i*-direction, and symbols ρ, μ, and p correspond to the density, molecular viscosity, and ensemble averaged pressures, respectively. The single term in the continuity equation represents the mass advection, while the first and second terms on the left-hand side in the momentum equation are the transient and momentum advection terms. The three terms on the right-hand side of the momentum equation are the pressure force, viscous term, and the Reynolds stress. The Reynolds stress term in Eq. (2) is unknown and contains the mean of the product of turbulent fluctuating velocities modeled by the Boussinesq approximation,

$$-\rho\left\langle u_i' u_j'\right\rangle = \mu_t\left(\frac{\partial u_i}{\partial u_j} + \frac{\partial u_j}{\partial u_i}\right) - \frac{2}{3}\left(\rho k + \mu_t\frac{\partial u_i}{\partial u_i}\right)\delta_{ij} \tag{3}$$

where μ_t and k represent the turbulent viscosity and turbulent kinetic energy. The Boussinesq approximation as shown by Eq. (3) relates the mean of the product of turbulent fluctuating velocities to a viscous stress term. In the Spalart-Allmaras model the kinetic energy is not calculated; therefore, the term with k in Eq. (3) is ignored. It should be noted that with this approximation the turbulent viscosity is assumed to be isotropic.

The Spalart-Allmaras turbulence model is then implemented to provide closure for the Navier-Stokes equations with the Boussinesq approximation. This model solves a single additional equation for the modified turbulent kinematic viscosity ν:

$$\frac{\partial}{\partial t}\left(\rho\tilde{\nu}\right) + \frac{\partial}{\partial x_i}\left(\rho\tilde{\nu}u_i\right) = G_\nu + \frac{1}{\sigma_{\tilde{\nu}}}\left\{\frac{\partial}{\partial x_j}\left[\left(\mu+\rho\tilde{\nu}\right)\frac{\partial\tilde{\nu}}{\partial x_j}\right] + C_{b2}\rho\left(\frac{\partial\tilde{\nu}}{\partial x_j}\right)^2\right\} - Y_\nu + S_{\tilde{\nu}} \tag{4}$$

where $\sigma_{\tilde{\nu}}$ and C_{b2} are constants and $S_{\tilde{\nu}}$ is the user defined source term. The production and destruction of turbulent viscosity are represented by $G_{\tilde{\nu}}$ and Y_ν, which are given in Fluent Manual (2005). Physically these terms account for the turbulent damping and production in the near wall region due to viscous damping and wall blocking. The turbulent dynamic viscosity is determined as follows,

$$\mu_t = \rho\tilde{\nu}f_{\nu 1} \tag{5}$$

where $f_{\nu 1}$ is a viscous damping function. Equation (5) connects the Spalart-Allmaras turbulence model back to the Boussinesq approximation of the Reynolds stress term. Although the turbulent viscosity and modified turbulent viscosities are the same throughout most regions of flow, the above relation accounts for the change in turbulent viscosity in viscous regions near walls. For more detailed explanation of Eqs. (4-5) and modeling of the production and destruction terms, the reader is referred to Fluent Manual (2005) or paper by Spalart and Allmaras (1991). The Spalart-Allmaras turbulence model has been used because it is computationally inexpensive and has been designed and validated for aerodynamic flows with adverse pressure gradients (Fluent, 2005) and performs well for wake flows and mixing layers (Rumsey and Ying, 2002).

This closed set of governing equations is solved numerically. The Finite Volume Method (FVM) is used to discretize and linearize the governing equations. This set of algebraic linear equations is then solved by Fluent 6.3. The segregated SIMPLE (Semi-Implicit Method for Pressure-Linked Equations) algorithm is implemented to modify the continuity equation into the needed pressure relation. The iterative nature of this procedure allows it to capture the non-linear nature of the physical situation while sequentially solving the governing equations. Stability in this iterative process is controlled by pressure and momentum relaxation factors which damp out numerical instabilities. The current research implements the 2nd order discretization scheme for pressure and the 3rd order MUSCL scheme for discretization of momentum and modified turbulent viscosity.

Generally, the use of a flap creates a separation zone behind the airfoil. As this separation zone increases in size, it can lead to unsteady effects such as vortex shedding. It has been observed that as the ground is approached, the separation zone behind the airfoil is restricted by the presence of the ground, yielding a limited separation region which is statistically stable and can be studied with a steady-state RANS solution. However, some flap geometries studied yield unsteady effects in the solution that prevent convergence. In these cases the Unsteady RANS (URANS) equations are used with the Spalart-Allmaras turbulence model. The validity of this approach has been questioned due to the possible averaging out of transient effects by the RANS technique. However, it has been shown that URANS can predict transient vortex shedding effects over many common geometries, such as a cylinder (Constantinescu et al., 2003) or a blunt airfoil (Doolan, 2007). In the current study, the unsteady flow structures play a minor role, so provided only

the time-averaged force coefficients are of interest, a complete resolution of the transient effects is not necessary (Ferziger and Peric, 1999). Therefore, the use of URANS with an appropriately small time step provides the necessary information, while avoiding the computational expense of Large Eddy Simulation (LES) or Detached Eddy Simulation (DES) for unsteady simulations.

Computational domain and flow conditions

The domain used to model flow around a wing with a flap extends 5 chords upstream of the airfoil, 12 chords downstream, 6 chords above, and the specified ground height below the airfoil. This domain is chosen since it captures all important physical phenomena; and it is similar, if not larger, than domains used in other WIG studies. As shown in Fig. 2, meshes created for this domain consist of two separate regions of quad elements. Initially a C-mesh surrounds the airfoil to provide an adequate mesh around the nose, while far from the airfoil an H-mesh is applied outside of the C-mesh to provide cells perpendicular to the flow. All meshes use the near wall technique and have been refined into the viscous sub layer, providing a first cell non-dimensional height of $y^+ \approx 1$ corresponding to a wall adjacent mesh size of approximately 10^{-5} chord lengths.

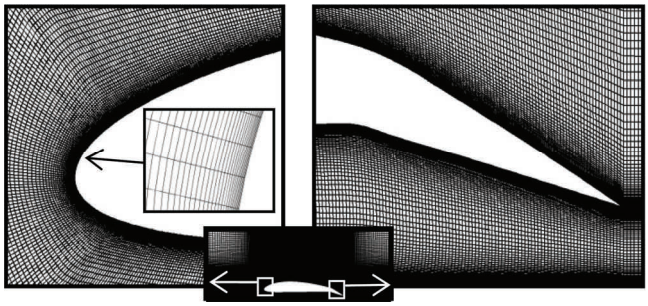

Fig. 2 Near-wall computational mesh of NACA 4412 ground-effect flight with plain flap at h/c=0.1, h_f/c=0.05, Re=10^6, and $\alpha = 2°$.

The general boundary condition at the ground has been chosen as a no-slip wall moving at the free stream velocity. This condition has been shown to provide a realistic model of the WIG flight, without introducing a ground boundary layer as on a stationary no-slip wall. The upstream and top boundaries are modeled as velocity inlets at the free stream conditions, while the downstream boundary is defined as a pressure outlet. Lastly, the airfoil surface is modeled as a no-slip wall. The above boundary conditions are used in all simulations unless specified otherwise.

In this work, Reynolds number, based on the wing chord and incident flow velocity, is selected to be 10^6 for most situations, while $Re = 10^7$ is also investigated for several cases. It is known that the dependence of results on Reynolds number above 5×10^5 becomes generally less significant and more predictable than below this value. With increasing Reynolds number above 10^6, minor increase of the lift coefficient and more substantial decrease of the drag coefficient are usually noticed (Hsiun and Chen, 2003).

RESULTS

Validation

Mesh independence studies were first completed for free-air flow without a flap and ground effect flow with a flap. The meshes chosen were refined to a point where the lift and drag coefficients ceased to significantly change with an increased number of cells.

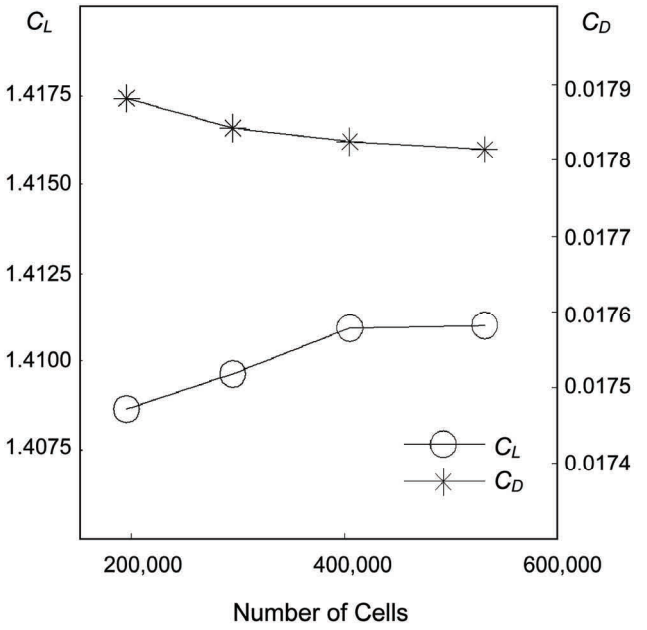

Fig. 3 Mesh independence study for NACA 4412 ground-effect flight with plain flap at h/c=0.1, h_f/c=0.05, Re=10^6 and $\alpha = 2°$.

Although the smallest grid size in this study is defined by the viscous sub-layer and is held constant, the 4 grids successively increase the number of cells between the airfoil and the ground from 100 to 250 in increments of 50. Solutions of the ground effect flow with a flap become nearly independent of the mesh density with 400,000+ cells as shown in Fig. 3. An estimated mesh converged solution is found using extrapolation (Ferziger and Peric, 1999) and lift and drag predictions are within 0.2% and 0.27% of the converged solution respectively. The small discrepancy between grids with 400,000+ cells and the extrapolated solution are more than adequate for the current design study. These metrics were used to assure that all meshes were of appropriate density (400,000+).

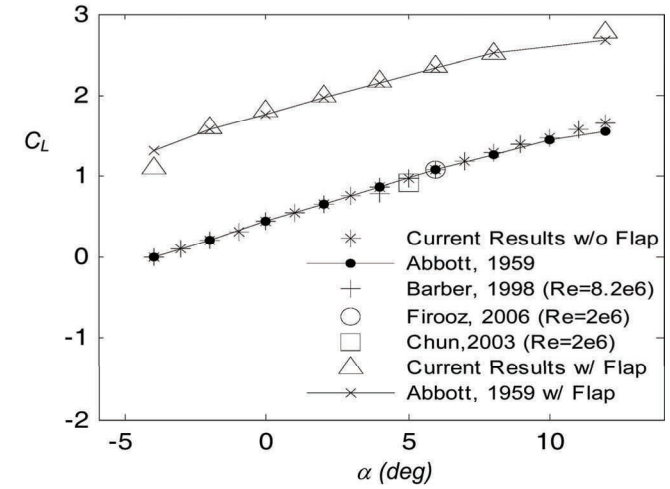

(a) lift coefficient

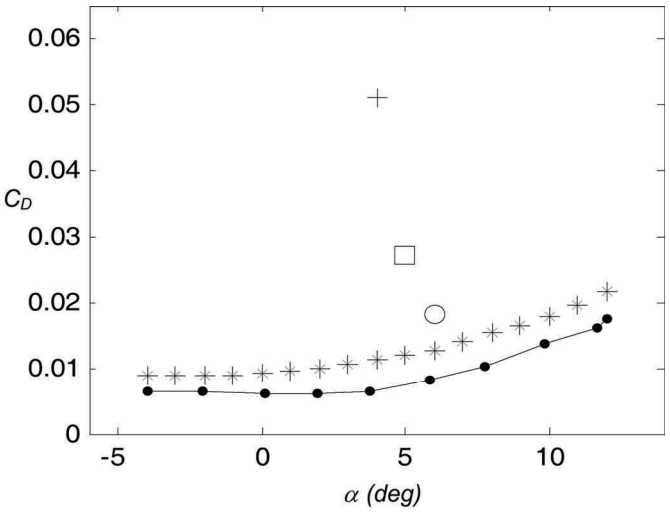

(b) drag coefficient

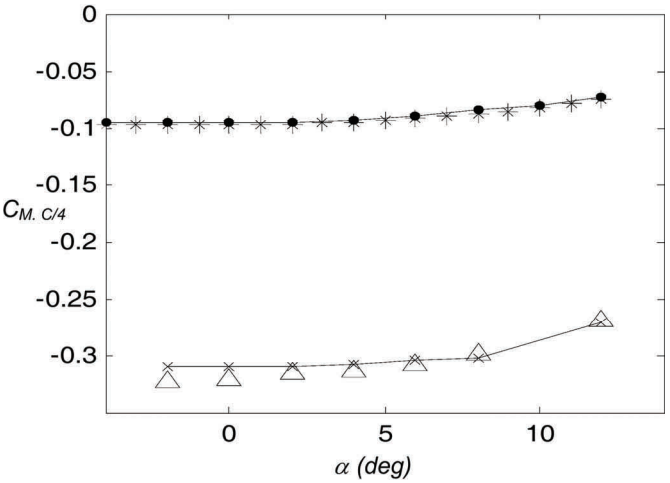

(c) moment coefficient.

Fig. 4 Experimental validation without ground effect at Re=6 ×10^6

To provide confidence in the current results, a validation has been completed against published results for similar studies. First, the NACA 4412 airfoil with and without a flap has been studied out of ground effect for comparison to two-dimensional experimental and numerical data. The additional flap consists of a 60° wedge (from horizontal) which is added to the airfoil at 80% chord just as shown by Abbott and Doenhoff (1959). Fluent code was used to compute the aerodynamic forces for several angles of attack at a Reynolds number of 6×10^6. Fig. 4 compares the numerical lift, drag, and quarter chord moment coefficients to the experimental and other numerical data.

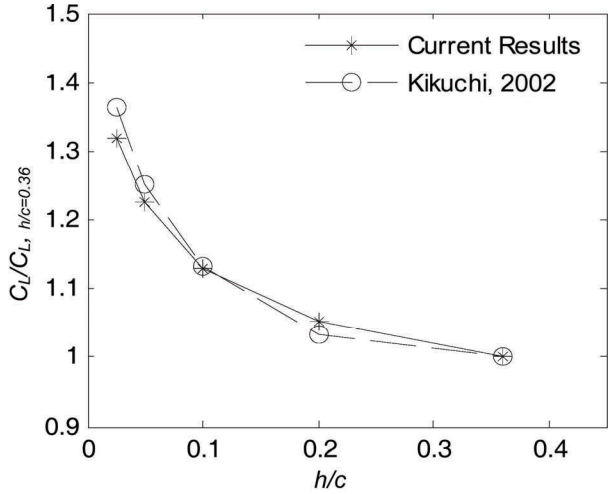

(a) experimental comparison at Re = 8.5×10^5

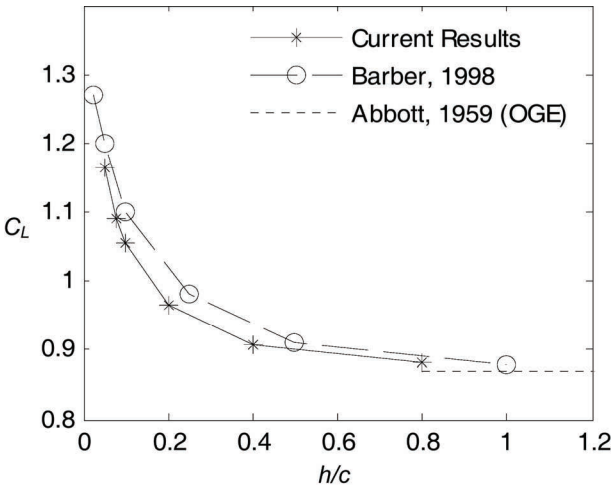

(b) numerical comparison at Re = 8.2×10^6

Fig. 5 Ground effect validation and comparison: (a) experimental comparison at Re = 8.5×10^5 and (b) numerical comparison at Re = 8.2×10^6. The dotted line shows the lift coefficient out of ground effect (Abbott and Doenhoff, 1959).

It is apparent that Fluent predicts lift and moment values similar to experiments in the broad intermediate range of attack angles. As the angle of attack approaches the extremities these results begin to deviate. This deviation is caused by the unsteady recirculation patterns that begin to shed at extreme angles. Similarly the numerical drag is also shown to correctly predict physical trends, while over predicting the magnitude of the drag force. This discrepancy in our modeling is found to be smaller than in other referenced studies. It is known that drag forces are difficult to accurately predict with numerical methods (Van Dam, 1999). Overall, the current modeling techniques used with Fluent predict the aerodynamic lift and moment closely in regions without dominant flow separation, while providing a correct drag trend that will suffice for the current study within the range of moderate lift coefficients.

Fluent modeling techniques have also been validated against available experimental and numerical published data for wing in ground flight without a flap. A normalized method is used to compare current numerical methods with experimental towing data for a Reynolds number of 8×10^5 and angle of attack of 6 degrees (Kikuchi et al., 2002) in Fig. 5a. Each set of data uses its respective lift coefficient $C_{L,\,0.36}$ at the largest experimental ground height h/c = 0.36 for normalization. It should be noted that both experimental and numerical data become weakly dependent of ground proximity above h/c = 0.36, yielding approximate out of ground values. It is believed that the deviation between the two lines in Fig. 5a is a consequence of possible experimental uncertainties in outdoor towing tests and relatively small Reynolds number. Fig. 5b shows current numerical results at Re = 8.2×10^6 compared to numerical data found in the literature. It is apparent that the tendencies shown in the ground effect regions are similar. However, the current data and numerical data from Barber et al. (1998) disagree on the magnitude of the aerodynamic forces in ground effect. Overall, these comparisons in ground effect provide a confidence in the ability to predict trends in the aerodynamic forces close to the ground.

Parametric calculations

A set of simulations were completed to determine the effects of ground height, flap deflection, attack angle, Reynolds number, and flap type for extreme ground effect with a trailing-edge flap. Non-dimensional ground heights of h/c = 0.05, 0.1, and 0.15 were studied for several flap deflections, including the undeflected case and limiting case with flap touching the ground. The above simulations have been repeated for the angle of attack 2° and 6° and Reynolds numbers 10^6 and 10^7. Most combinations have been run with a plain flap, while some selected cases at h/c = 0.05 and 0.1 have also been calculated with a split flap for comparison.

An assessment of different ground boundary conditions and turbulence models is presented first. Fig. 6 shows the pressure distribution comparison between fixed, moving, and symmetry ground boundary conditions. It is apparent that compared to moving and symmetry conditions, the fixed ground boundary condition provides a significantly smaller pressure below the airfoil. This effect is due to a boundary layer created between the fixed ground and free stream flow, reducing flow beneath the airfoil and diminishing the pressure ram effect. This boundary layer is dependent on the upstream size of the computational domain, as size of upstream domain increases a larger boundary layer will result. In this study the moving ground boundary condition is used as it is presents the most physically reasonable condition with the no-slip ground set to move at the same speed as the free stream flow.

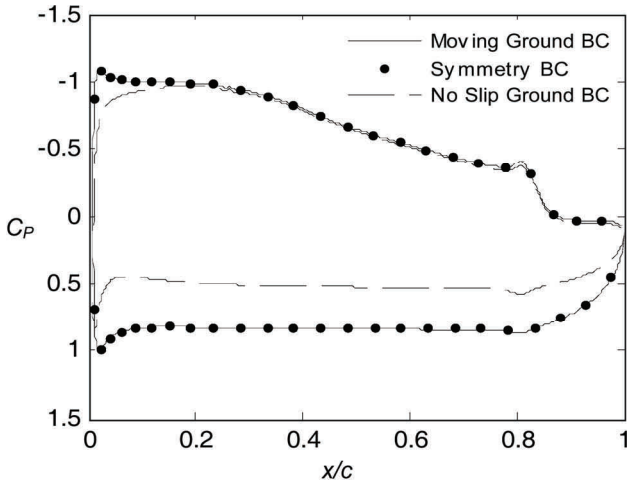

Fig. 6 Pressure distribution for various ground boundary conditions at h/c=0.1, h_f/c=0.05, Re=10^6 and α = 2°.

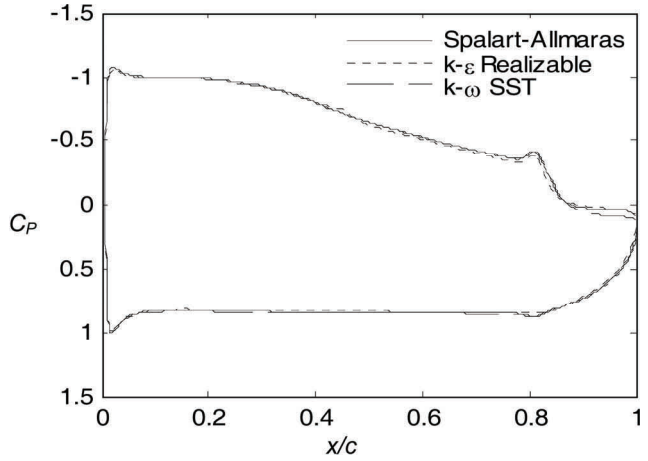

Fig. 7 Pressure distribution for various RANS turbulence models at h/c=0.1, h_f/c=0.05, Re=10^6 and α = 2°.

Similarly, Fig. 7 shows a comparison of pressure distributions for three different RANS turbulence models available in Fluent. The Spalart-Allmaras, k-ε Realizable, and k-ω SST models are all used to determine flow for a case with ground height of h/c = 0.1, flap height h_f/c = 0.05, α = 2°, and Reynolds number of 10^6. All models similarly predict the distributions on the pressure side of the airfoil along with the suction peak above the airfoil. Variation can be seen on the upper surface of the flap where separation begins to occur.

However, these variations are of a small scale and have little impact on the aerodynamic forces on the airfoil. Therefore, as mentioned above, the Spalart-Allmaras turbulence model is used for all following simulations and other models are expected to behave similarly.

The flow field is first presented in Fig. 8 with the non-dimensional velocity magnitude contours (local velocity / vehicle speed U) for the case of h/c = 0.1, α = 2°, and Re = 10^6 for several different plain flap heights. Fig. 8a shows the airfoil without flap deflected, Fig. 8b presents a flap height of h_f/c = 0.05, and finally Fig. 8c is the limiting case where and finally Fig. 8c is the limiting case where the tip of the flap is touching the ground.

(a) h_f/c=0.1

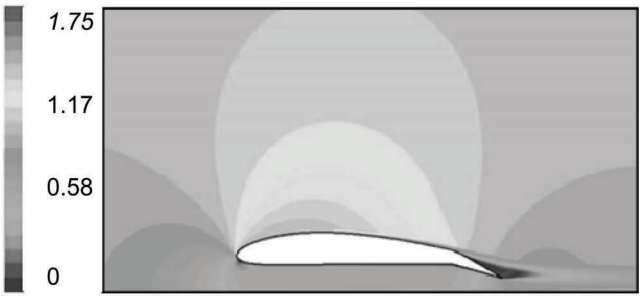

(b) h_f/c=0.05

(c) h_f/c=0.0

Fig. 8 Non-dimensional velocity magnitude contours at h/c=0.1, Re=10^6 and α=2°.

As the flap is deployed, increasing amounts of flow are trapped underneath the airfoil, significantly reducing the flow speed in this region. With a reduction in the flow underneath the airfoil, larger amounts of flow are forced over the nose of the airfoil increasing the flow speed on the suction side. As the flap is deflected, the stronger adverse pressure gradient on the upper side of the airfoil, coupled with the jet type flow through the diminishing gap at the trailing edge, leads to flow separation on the flap surface. In the limiting case when the flap touches the ground, all flow underneath the airfoil is trapped, creating a large recirculation zone and directing all incident flow above the airfoil. It is observed that as the flap is deflected, the recirculation zone grows on the upper surface of the flap until the limiting case where a large statistically stable recirculation region is created between the flap and the ground. The limiting case flap recirculation is shown in Fig. 9.

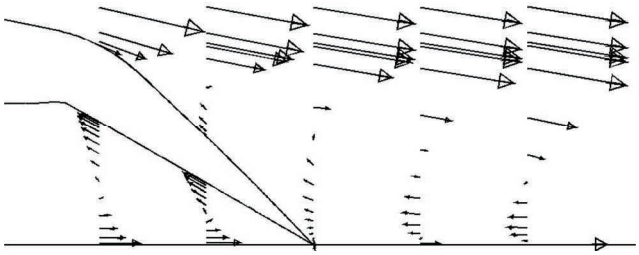

Fig. 9 Velocity vectors of trailing edge flap recirculation at h/c=0.1, h_f/c=0.0, Re=10^6 and α = 2°.

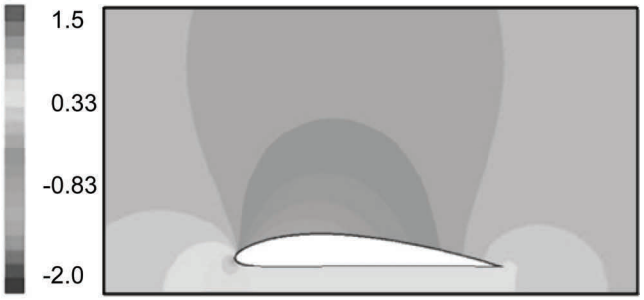

(a) h_f/c=0.1

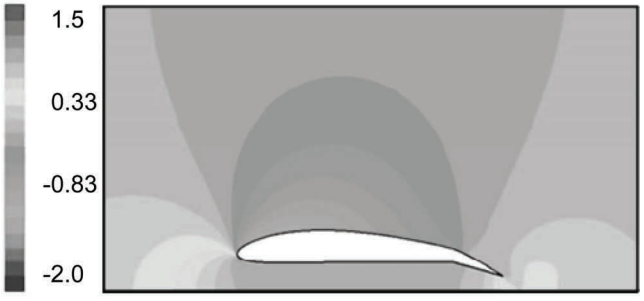

(b) h_f/c=0.05

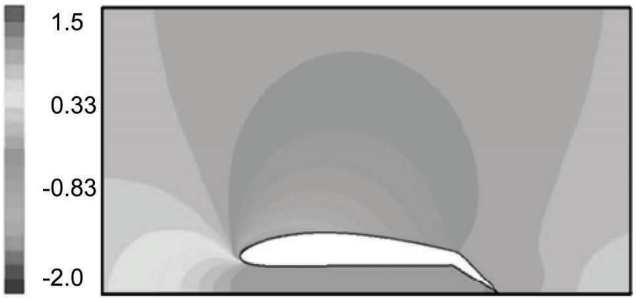

(c) h_f/c=0.0

Fig. 10 Pressure coefficient contours at h/c=0.1 with Re=10^6 and α=2°.

Similarly, the pressure coefficient contours are determined for the same case and are shown in Fig. 10 for flap deflections of h_f/c = 0.1, 0.05, and 0. As the flap is deployed, it is observed that the slowdown and entrapment of flow leads to a significant pressure recovery beneath the airfoil. It appears that the largely augmented suction peak on the upper nose of the airfoil is due to the increased flow over the suction surface, caused by the increased pressure beneath the airfoil forcing large amounts of flow over the airfoil. It is found that the pressure underneath the airfoil and the suction peak continue to increase until the limiting case where the flap is touching the ground. In this limiting case nearly all flow underneath the airfoil is stagnated, creating a high-pressure zone, while flow forced over the nose creates the beneficial low pressure zone above the airfoil.

Further insight into the flow behavior is obtained from Fig. 11 illustrating the pressure distribution of the same case with h/c = 0.1, α = 2°, and Re = 10^6 for varying plain flap heights. As the pressure and velocities implied, the pressure underneath the airfoil and the suction peak both increase as the flap is deflected. The general area in between the pressure and suction curves is an indicator for the lift force. Therefore, it is apparent that as the flap is deflected the lift force of the airfoil should significantly increase. When the flap is deflected to the ground the pressure coefficient is shown to approach to or even exceed one. It can be noted that the theoretical maximum for the pressure coefficient is one for the completely stagnated flow and two for the ideally reversed flow. The conflicting boundary conditions, which define the flap trailing-edge point as a part of a stationary wing profile and a moving ground boundary, may introduce inaccuracy in the solution near this point. However, the region where flow is influenced by this effect is rather limited and, therefore, has negligible effect on the force coefficients.

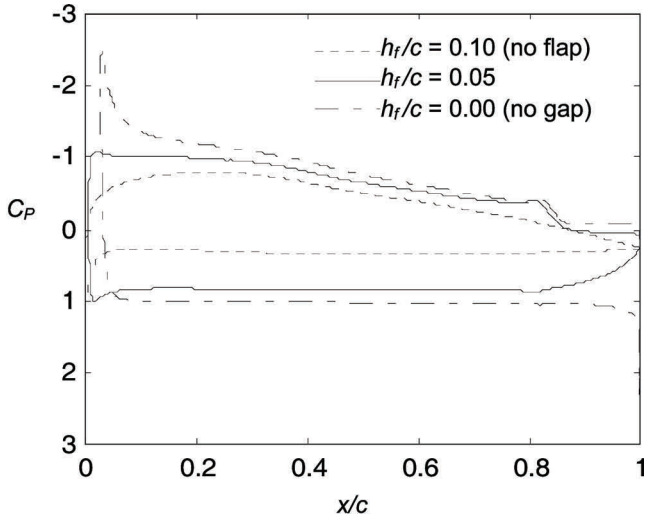

Fig. 11 Pressure distribution as flap is deflected in ground effect at h/c=0.1, Re=10^6 and α = 2°.

The aerodynamic lift coefficient, drag coefficient, quarter-chord moment coefficient, and lift-to-drag ratio in extreme ground effect flight with a flap are shown in Fig. 12 for α = 2° and Re = 10^6. As expected, the lift increases when the flap is deflected for all ground heights (Fig. 12a). However, the amount of lift augmentation due to the flap appears to lessen as the flap deflection is increased. Therefore, deflecting the flap in extreme ground effect is very effective with small deflections, while the benefit of further deflecting the flap will yield a diminishing gain. Another interesting trend takes place as the ground height h increases with a specified flap height h_f. In this situation the curves for the greater ground heights are above those of lesser ground heights. This lift increase can be explained due to the larger amount of flow which may be trapped beneath the airfoil at a greater ground height with the same distance between the flap and the ground. Lastly, insight can be gained on the situation where an airfoil holds a constant flap deflection, y_f, while approaching the ground. Similar to the ground proximity flight without a flap, with a specified flap deflection the lift is shown to increase as the airfoil approaches the ground. Overall, as shown in the out of ground case the use of a flap in the extreme ground effect increases the lift of the airfoil up to the limiting case where the flap is touching the ground.

Similarly, the drag coefficient is shown to increase with flap deflection in Fig. 12b. This significant drag increase appears to be caused by two contributing pressure drag forces. As shown in Fig. 11 the pressure underneath the airfoil increases as the flap is deflected. This increase coupled with vertical projection of the deflected flap creates an increasing area perpendicular to the flow resulting in a much greater drag force in the flow direction. In addition to this drag increase, the use of a flap has been shown to increase the separation on the upper surface of the flap providing a low-pressure zone behind the flap and further increasing the pressure drag. Overall, with the same flap deflection, y_f, the ground height appears to have little effect on the drag force, as the large pressure drag due to the flap appears to dominate.

Fig. 12c presents the quarter-chord moment coefficient as the flap is deflected in extreme ground effect. The moment coefficient is defined as the moment at the quarter chord as shown in Fig. 1 divided by the free stream dynamic pressure, airfoil surface area, and chord. As the flap is deflected at a specified ground height h, the nose down pitching moment is shown to increase up until the limiting case where flap is touching the ground. This increase in nose down pitching moment is explained by the larger pressure beneath the airfoil acting against the increased area of the blunt flap. Similarly, as the airfoil approaches the ground with constant flap deflection y_f, the nose down pitching moment also increases as pressure beneath airfoil is augmented in ground effect. However, as the airfoil approaches the ground while holding a constant flap height h_f, the nose down pitching moment decreases, as smaller amounts of flow are trapped beneath the airfoil.

The lift-to-drag ratio, which represents the aerodynamic efficiency of flight, is shown in Fig. 12d. This characteristic has been one of the selling points of ground effect vehicles, since near the ground an increase in lift and decrease in drag lead to an improvement in the aerodynamic efficiency. To

this point the use of a flap in ground proximity has shown competing contributions to the lift-to-drag ratio: the lift is augmented by a flap, while the pressure drag largely increases with the implementation of a flap. In the current study it is observed that small deflections of the flap, where the lift is strongly augmented, leads to an increased lift-to-drag ratio. As the flap is further deflected the pressure drag begins to dominate and the lift-to-drag ratio drops significantly lower than the case of undeflected flap in ground-effect. The lift-to-drag ratio appears to generally reach a maximum with the flap deflected 2.5% of the chord, and continues to be greater than the undeflected flap until a flap deflection of approximately 5% of the chord is reached. Overall, it is shown that the use of a small plain flap deflection in ground effect can increase the aerodynamic efficiency and provide an improved operating region for the considered angle of attack.

Results of the selected split flap simulations are also shown in Fig. 12. Differences in the lift and moment coefficients between split and plain flaps are found to be minimal, with the split flap providing slightly higher lift in the limiting case with the flap touching the ground. The drag coefficient is also predicted similarly. There are minimal differences until the limiting case where the split flap geometry predicts a significantly smaller drag. This reduction in drag may be a result of the smaller separation zone behind the split flap as compared to the plain flap. The split flap does not deflect the rear of the airfoil as in the plain flap case. Instead, an additional flap is added as an attachment to the existing undeflected airfoil. As expected from the lift and drag behavior, the lift-to-drag ratio is very similar to the plain flap data until the limiting case is reached. At this point the split flap provides a much higher lift-to-drag ratio, resulting in improvements over the plain flap in the limiting case with flap touching the ground.

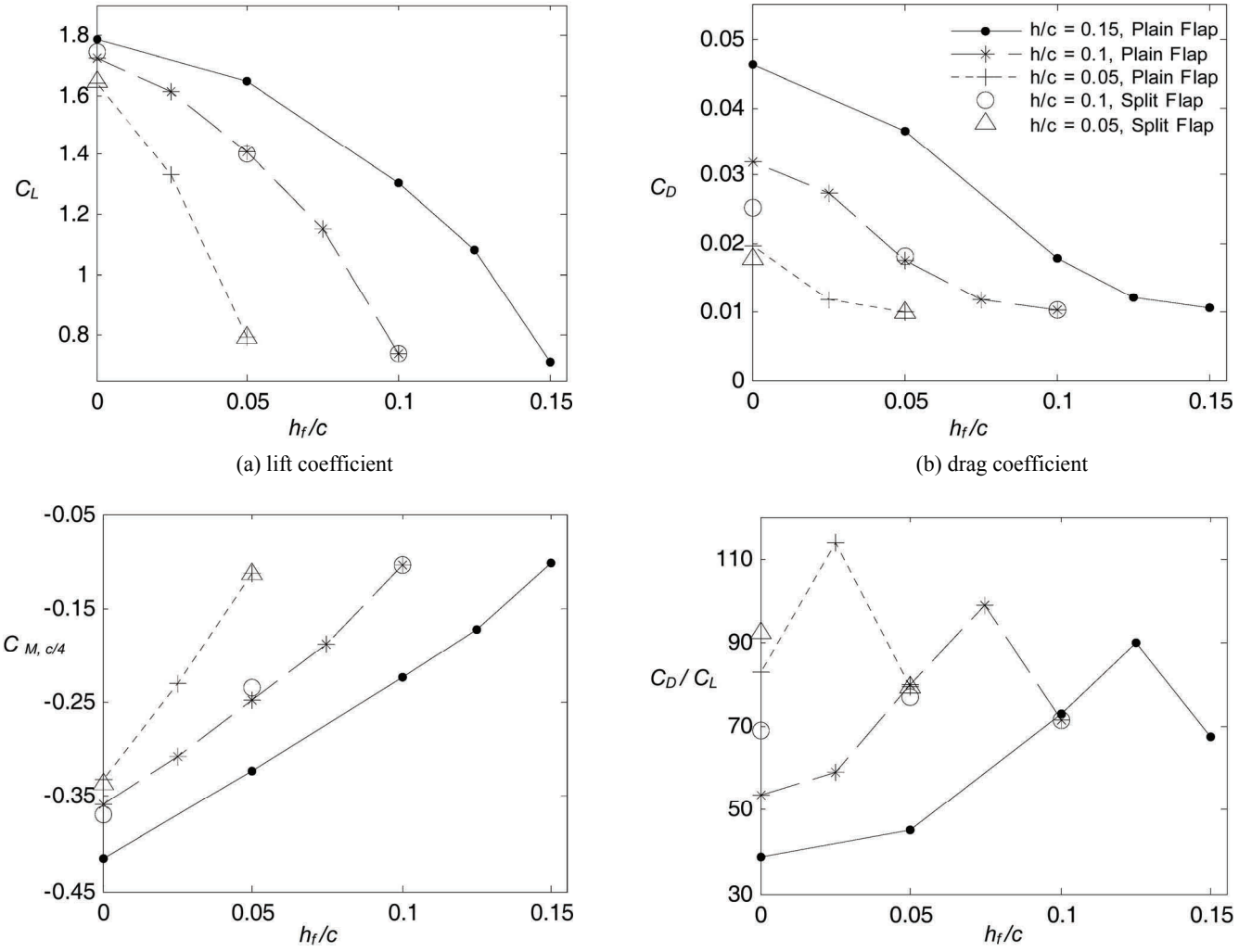

(a) lift coefficient

(b) drag coefficient

(c) quarter-chord moment coefficient

(d) lift-to-drag ratio

Fig. 12 Aerodynamic trends as flap is deflected while approaching the ground at Re=10^6, and α=2°.

Results for a plain flap with constant flap deflection y_f/c = 0.05 at attack angles 2° and 6° and Reynolds number 10^6 are shown in Fig. 13. As theoretically expected, the lift and drag increase as the angle of attack is increased. However, as the ground is approached, the lift augmentation gained by increasing angle of attack is reduced. This is apparent for α = 2° and 6° as there is a large difference in lift values out of ground (plotted at h/c=1), while as airfoil with flap approaches extreme ground proximity the curves approach each other, resulting in a smaller lift benefit with increasing attack angles in ground effect. It is also noticed that in the distant ground effect region, h/c ~ 0.5, the airfoil with flap deflected obtains a lesser lift than the out of ground flap case, which is similar to previous observations (Steinbach and Jacob, 1991). As the airfoil further approaches the ground, the flap is shown to then provide improved aerodynamic properties. Unlike the lift, the drag is shown to be significantly higher for the out of ground case, while reducing in ground proximity. Overall, the lift and drag increase with angle of attack, while in some regions the use of flap in weak ground effect yields a smaller lift than in the out of ground case.

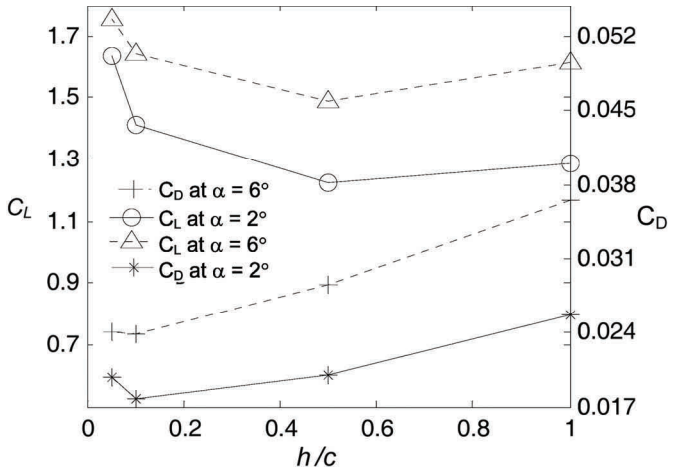

Fig. 13 Effects of angle of attack with constant flap deflection of y_f/c = 0.05 and Re=10^6 for plain flap. Data plotted at h/c = 1 correspond to values at h/c = ∞.

Reynolds number effects on ground proximity flight with a flap are also of practical importance. The pressure distributions for h/c = 0.1, α = 2°, while comparing Re = 10^6 and Re = 10^7 are shown in Fig. 14. Pressure distributions for both Reynolds numbers appear to behave very similarly. The pressures below the airfoil are shown to slightly increase as the Reynolds number increases. Similarly, the suction pressures above the airfoil are also slightly increased.

Fig. 15 presents the effect of Reynolds number on the lift and drag coefficients for a ground height h/c = 0.1, flap height h_f/c = 0.05, and α = 2°. As expected, the minimal changes in pressure distributions have only led to a very small lift increase with increased Reynolds number. On the other hand, the drag coefficient is shown to significantly decrease with increased Reynolds number. This effect can be related to behavior of the skin-friction coefficient in turbulent flow which decreases with the Reynolds number. Overall, an increase in Reynolds number is shown to have small influence on the aerodynamic effects due to flap use in extreme ground effect.

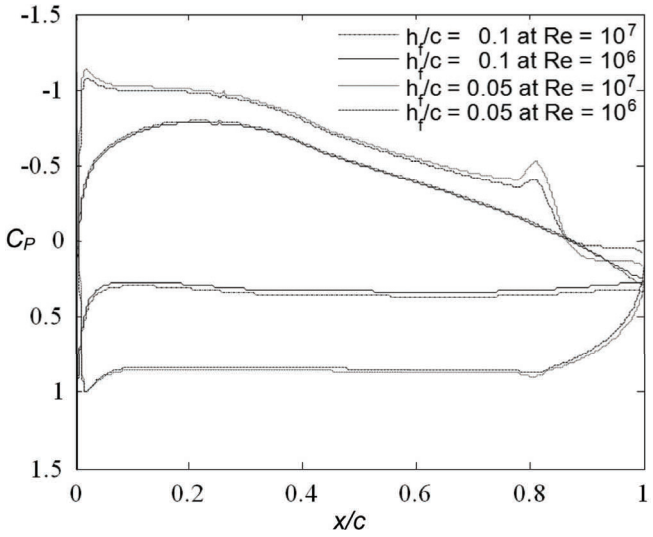

Fig. 14 Pressure distribution for varying Reynolds numbers at h/c = 0.1 and α = 2°.

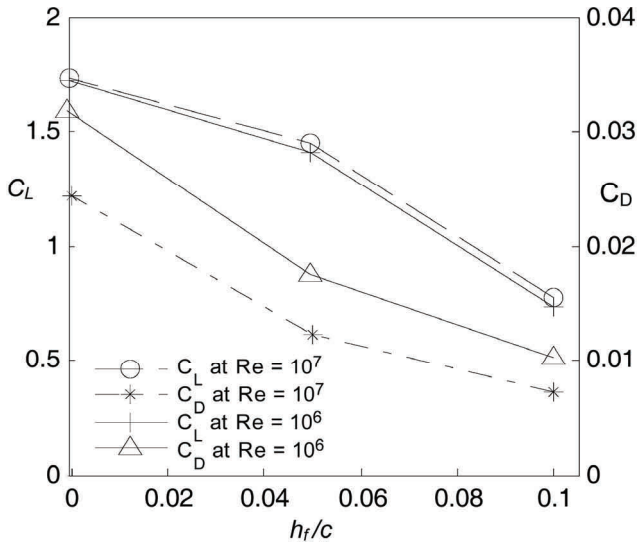

Fig. 15 Reynolds number effects on lift and drag coefficients at h/c = 0.1 and α = 2°.

SUMMARY AND CONCLUSIONS

The turbulent flow around an airfoil in extreme ground effect with a flap was studied with computer program Fluent, a finite volume code using the segregated SIMPLE solver. The equations governing the two-dimensional, incompressible

flow are the RANS equations, with the Spalart-Allmaras turbulence model implemented to provide closure. With the addition of a flap in extreme ground proximity the effects of flap deflection, ground height, flap type, angle of attack, and Reynolds number have been studied. Conclusions from the results provide insight in the aerodynamic characteristics of the flow, as well as beneficial flight regimes for ground proximity flight with a flap.

- The numerical methods used are validated through a mesh independence study along with comparisons to experimental and numerical data for free air flight with and without a flap, and ground effect flight without a flap. The current results predict the aerodynamic coefficients closely in free air flight, while capturing the trends of wing-in-ground flight similar to other studies. These validations provide confidence in the current modeling techniques. However, a full validation in extreme ground effect cannot be completed until accurate experimental data in the appropriate WIG operating range are obtained.
- As flap is deflected, the flow is trapped beneath the airfoil, leading to decrease of flow velocities and build-up of the pressure below the airfoil. Simultaneously, the increasing adverse pressure gradient with flap deflection yields a larger flow separation behind the flap. In the limiting case with the flap touching the ground, flow underneath the airfoil is nearly stagnated creating a recirculation zone underneath the airfoil, while forcing a larger amount of flow over the nose. Also, near the trailing edge with flap touching the ground a large statistically stable recirculation zone develops at the upper surface of the flap and the downstream portion of the ground.
- In extreme ground effect and small attack angles, the lift coefficient increases as the flap is deflected for all ground heights, though the amount of lift augmentation due to the flap appears to lessen as the flap deflection increases. A lift increase is also shown while holding the flap height h_f constant and increasing the ground height h, which is explained by the ability to trap more flow beneath the airfoil. Lastly, with the flap deflection held constant, the lift also increases as the airfoil approaches the ground, similar to the wings without a flap suitable for ground-effect operations, i.e., where lift increases with decreasing ground height h.
- Drag coefficient significantly increases as the flap is deflected. This increase is due to larger pressure underneath the airfoil yielding increased pressure drag, along with the growing separation zone on the upper surface of the flap. Ground proximity shows minimal effects on drag as the flap addition dominates.
- With small flap deflection the lift-to-drag ratio is found to be significantly augmented (h_f/c = 0.025). However, as flap is deflected past h_f/c = 0.05, the increased pressure drag then dominates and yields lower lift-to-drag ratios than the case without a flap.
- Differences in performance between split and plain flaps appear to be minimal for most flow geometries. However, in the limiting case with the flap touching the ground a split flap is shown to better contain the separated flow behind the flap which significantly reduced the drag and increased the lift-to-drag ratio.
- As Reynolds number is increased a small lift augmentation is shown, while at the same time the drag reduces more substantially, mainly due to decrease in the skin-friction coefficient in turbulent flow. Overall, changes in Reynolds number appear to have minimal effects on the flap addition in extreme ground effect.
- Lift and drag are also shown to increase with angle of attack. However, the changes in angle of attack with a flap out of ground effect show much greater lift augmentation than in ground effects, implying that in extreme ground effect with flap deflected the effects of angle of attack are reduced.
- A beneficial flight regime appears to be obtainable in ground effect flight for an airfoil with a relatively flat bottom surface, such as the NACA 4412, using simple flap mechanization, such as the implementation of split or plain flaps. In extreme ground effect it is shown that the use of small flap deflections significantly increases the lift while increasing the drag to smaller extent. With flap deflected up to y_f/c = 0.05 an increase in the lift-to-drag ratio is found, effectively improving ground proximity flight with the use of a flap.

REFERENCES

Abbott, I. and Doenhoff, A., 1959. *Theory of wing sections*. Dover Publications, New York.

Barber, T. Leonard, E. and Archer, D., 1998. Appropriate CFD techniques for the prediction of ground effect aerodynamics. *Proceedings of Workshop 'WISE up to ekranoplan GEMs'*, University of New South Wales, Sydney, Australia.

Chun, H. and Chang, R., 2003. Turbulence flow simulation for wings in ground effect with two ground conditions: fixed and moving ground. *International Journal of Maritime Engineering*, 145, pp.51-68.

Constantinescu, G. Chapelet, M. and Squires, K., 2003. Turbulence modeling applied to flow over a sphere. *AIAA Journal*, 41(9), pp.1733-1742.

Doolan, C., 2007. Numerical simulation of a blunt airfoil wake using a two-dimensional URANS approach. *Proceedings of 16th Australasian Fluid Mechanics Conference*, University of Queensland, Australia.

Ferziger, J. and Peric, M., 1999. *Computational Methods for Fluid Dynamics*. Springer, New York.

Firooz, A. and Gadami, M., 2006. Turbulence flow for NACA 4412 in unbounded flow and ground effect with different turbulence models and two ground conditions: fixed and moving ground conditions. *Proceedings of International Conference on Boundary and Interior Layers*, Gottingen, Germany.

Fluent, 2005. *Fluent 6.2: Users manual*.

Gallington, R.W., 1987. Power augmentation of ram wings. *Proceedings of Conference on RAM Wings and Ground Effect Craft*, RINA, London, UK.

Gallington, R.W. Chaplin, H.R. and Krause, F.H., 1976. Recent advances in Wing-in-Ground effect vehicle technology. *Proceedings of AIAA/SNAME Advanced*

Marine Vehicles Conference, Arlington, VA, USA, AIAA paper No.76-874.

Hayashi, M. and Endo, E., 1978. Measurement of flow fields around an airfoil section with separation. *Transactions of the Japan Society for Aeronautical and Space Sciences,* 21, pp.69-75.

Hirata, N. and Hino, T., 1997. Investigation of a three-dimensional power-augmented ram wing in ground effect. *Proceedings of 35th Aerospace Sciences Meeting & Exhibit*, AIAA, Reno, USA, AIAA paper No.97-0822.

Hsiun, C. and Chen, C., 1996. Aerodynamic characteristics of a two-dimensional airfoil with ground effect. *Journal of Aircraft*, 33(2), pp.386-392.

Huffman, J.K. and Jackson, C. M. Jr., 1974. Investigation of the static lift capability of a low-aspect-ratio wing operating in a powered ground-effect mode. *NASA Technical Memorandum* X-3031.

Katz, J. and Plotkin, A., 1991. *Low-Speed Aerodynamics – from Wing Theory to Panel Methods*. McGraw-Hill, New York.

Kikuchi, M. Hirano, K. Yuge, T. Iseri, K. and Kohma, Y., 2002. Measurement of aerofoil characteristics by method of towing. *Transactions of the Japan Society of Mechanical Engineers*, 68(676), pp.3378-3385.

Kirillovykh, V.N. and Privalov, E.I., 1996. Transport amphibious platforms: a new type of high-speed craft. *Proceedings of Workshop on Ekranoplans and Very Fast Craft*, University of New South Wales, Sydney, Australia.

Kornev, N.V. and Matveev, K.I., 2003. Complex numerical modeling of dynamics and crashes of Wing-in-Ground vehicles. *Proceedings of 41st Aerospace Sciences Meeting & Exhibit*, Reno, USA, AIAA paper No. 2003-0600.

Krause, F.H., 1977. Evaluation of a Power-Augmented-Ram wing operating free in heave and pitch over water. DTNSRDC Report ASED-385.

Matveev, K.I., 2008. Static thrust recovery of PAR craft on solid surfaces. *Journal of Fluids and Structures*, 24(6), pp. 920-926.

Rozhdestvensky, K.V., 2000. *Aerodynamics of a Lifting System in Extreme Ground Effect*. Springer, Heidelberg, Germany.

Rozhdestvensky, K.V., 2006. Wing-in-Ground effect vehicles. *Progress in Aerospace Sciences*, 42, pp.211-283.

Rumsey, C.L. and Ying, S.X., 2002. Prediction of high lift: review of present CFD capabilities. *Progress in Aerospace Sciences*, 38(2), pp.145-180.

Serebrisky, Y.M. and Biachev, S.A., 1946. Wind-tunnel investigation of the horizontal motion of a wing near the ground. *NACA Technical Memorandum* 1095.

Spalart, P. and Allmaras, S., 1991. A one-equation turbulence model for aerodynamic flows. *Proceedings of 29th Aerospace Sciences Meeting*, AIAA Paper No. 92-0439.

Steinbach, D. and Jacob, K., 1991. Some aerodynamic aspects of wings near ground. *Transactions of the Japan Society for Aeronautical and Space Sciences*, 34(104), pp.56-70.

Van Dam, C.P., 1999. Recent experience with different methods of drag prediction. *Progress in Aerospace Sciences*, 35(88), pp.751-798.

Wu, C.K. and Rozhdestvensky, K.V., 2001. High-Reynolds-number flow computations for wings in ground effect. *Proceedings of 6th International Conference on Fast Sea Transportation*, Southampton, UK.